ISBN: 978-3-95450-216-5 doi:10.18429/JACoW-eeFACT2018-MOXBA01

CHALLENGES FOR CIRCULAR e+e− COLLIDERS*

Frank Zimmermann†, CERN, Geneva, Switzerland

Abstract

This paper sketches the glorious past and the tantalizing future of circular e+e− colliders, highlighting some of the key issues.

HISTORY

Circular e+e− Colliders can look back at a 50-year success story, illustrated in Fig. 1. The collider with the highest energy so far was LEP/LEP2. LEP had a circumference of about 27 km, and was in operation from 1989 to 2000. During this time it delivered an integrated luminosity of 1000 pb^{-1}. LEP2 reached a maximum c.m. energy of 209 GeV, a maximum synchrotron radiation power of 23 MW, and a critical photon energy close to 1 MeV. A further important step forward was made by the two B factories, PEP-II and KEKB; see Fig. 2. They established collider operation at very high beam current (well above 1 Ampere per beam), world record luminosities, and top-up injection as a routine mode of operation. Another machine, DAΦNE, demonstrated the merits of crab-waist collisions, with a small β_y^* and large vertical beam-beam tune shift (Fig. 3).

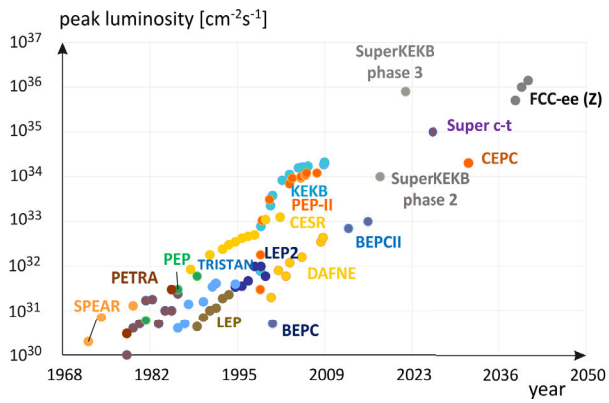

Figure 1: Peak luminosity of circular e+e− colliders as a function of year — for past, operating, and proposed facilities including the Future Circular Collider (Historical data courtesy of Y. Funakoshi).

NEXT STEPS

The next big step will be the SuperKEKB (Fig. 4), whose beam commissioning started in 2016. SuperKEKB will operate with a "nanobeam collision scheme" (similar to the crab waist, but without any crab-waist sextupoles). It features a design beam lifetime of no more than 5 minutes, and a vertical IP beta function β_y^* of only 0.3 mm.

* This work was supported by the European Commission under the HORIZON 2020 project ARIES no. 730871.
† frank.zimmermann@cern.ch

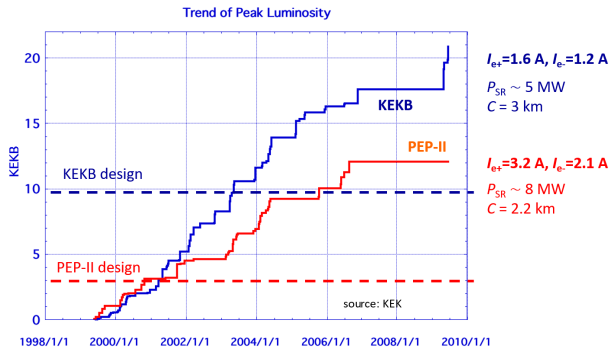

Figure 2: Peak luminosity of PEP-II and KEKB as a function of year along with the design luminosity, and a few key parameters.

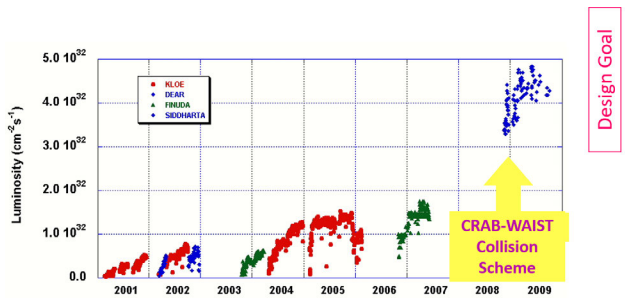

Figure 3: DAΦNE peak luminosity versus time, and the step increase in 2008/9 thanks to the introduction of crab-waist collisions (P. Raimondi, M. Zobov).

The proposed future highest-energy highest-luminosity e+e− colliders build on past successes and lessons. LEP has pushed high-energy beam operation and experienced synchrotron-radiation effects like those expected for FCC-ee $t\bar{t}$ running. The B-factories KEKB and PEP-II have operated with high beam currents, as needed for the FCC-ee Z pole operation. They have also established the top-up injection mode. DAΦNE has demonstrated the crab waist collision scheme. The Super B factory SuperKEKB will explore the operation with extremely low β_y^*. The SLC, KEKB and SuperKEKB have demonstrated the positron source operation at high intensity. Finally, HERA, LEP, and RHIC have delivered important lessons on spin gymnastics, spin-orbit matching and operating storage rings with polarized beams.

The next machines are combining all the recently established concepts, as indicated in Fig. 5. Figure 6 compares the resulting tantalizing performance reach of FCC-ee with other proposed future colliders.

ISBN: 978-3-95450-216-5 doi:10.18429/JACoW-eeFACT2018-MOXBA01

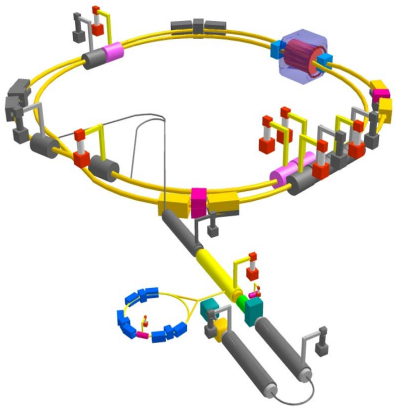

Figure 4: Schematic of SuperKEKB (K. Oide et al.).

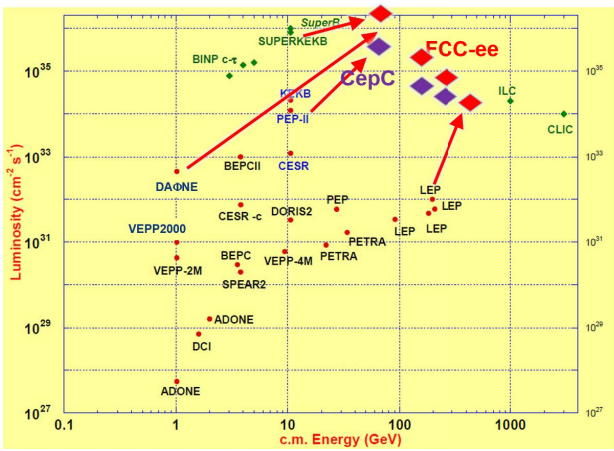

Figure 5: Past, present and future collider landscape: combining recent, novel ingredients yields extremely high luminosity at high energies (Marica Biagini).

FEASIBILITY AND OPTIMIZATION

Already in the mid 1970's it was observed that "an e^+e^- storage ring in the range of a few hundred GeV in the centre of mass can be built with present technology." [and] "...would seem to be ... most useful project on the horizon." [1]. In the same reference [1] it was shown that 365 GeV c.m. energy corresponds to a cost-optimized circumference of about 100 km, thereby validating the much more recent FCC-ee design choice.

Table 1 shows that the FCC-ee machine faces quite different requirements in its various modes of operation. For example, on the Z pole FCc-ee is an Ampere-class storage ring, like PEP-II, KEKB and DAΦNE, with a high beam current, but a low RF voltage, of order 0.1 GV. For the $t\bar{t}$ mode, the beam current is only a few mA, as for the former LEP2, while an RF voltage above 10 GV is required. In both cases a total of 100 MW RF power must be constantly supplied to the two circulating beams.

Three sets of RF cavities are proposed to cover all operation modes for the FCC-ee collider rings and booster. (1) For

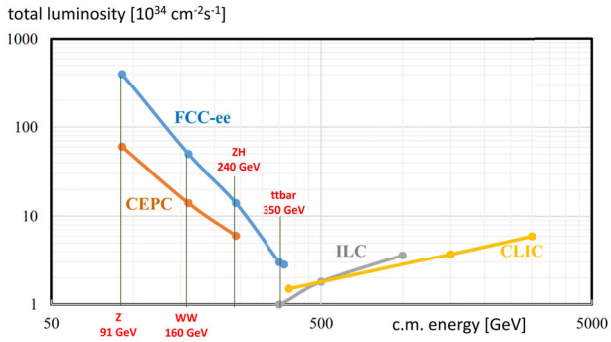

Figure 6: Total luminosity forecast for four proposed future e^+e^- colliders as a function of c.m. energy.

the high intensity operation (Z, FCC-hh) 400 MHz monocell cavities (4 per cryomodule) based on Nb/Cu thin-film techology at 4.5 K are proposed; (2) for higher energy (W, H, $t\bar{t}$) 400 MHz four-cell cavities (4 per cryomodule) again based on Nb/Cu technology at 4.5 K, and (3), finally for the $t\bar{t}$ machine a complement of 800 MHz five-cell cavities (again 4 per cryomodule) based on bulk Nb at 2 K. The installation sequence (Fig. 7) is comparable to the one of LEP, where about 30 cryomodules were installed per shutdown.

Table 1: RF voltage, number of bunches, and beam current for the four modes of FCC-ee operation

mode	RF voltage [GV]	# bunches	current [mA]
Z	0.1	16640	1390
W	0.44	2000	147
ZH	2.0	393	29
$t\bar{t}$	10.9	48	5.4

HIGH BEAM CURRENT

High current, short bunches, and a large ring can give rise to higher-order-mode (HOM) losses and single-bunch instabilities. HOM heat loads can easily destroy beamline elements, as is illustrated in Fig. 8 with photographs from PEP-II [3]. The HOM power is given by [3]

$$P_{\mathrm{HOM}} = t_{\mathrm{bs}} k_{||} I_b^2 \,, \qquad (1)$$

where I_b denotes the beam current, t_{bs} the bunch spacing, $k_{||}$ the loss factor, and I_b the total beam current. HOM mitigation calls for shielded, damped, suitably designed beamline components. The HOMs in the RF cavities restrict the possible bunch spacings [4]. As a design criterion, the total HOM energy loss should stay much smaller than the energy loss from synchrotron radiation.

Novel thin NEG coatings can simultaneously ensure: acceptable vacuum conditions (good pumping properties), suppression of electron cloud build up (low secondary emission yield), and a longitudinal single-bunch impedance below the threshold of the microwave instability [5]; see Fig. 9. Figure

ISBN: 978-3-95450-216-5 doi:10.18429/JACoW-eeFACT2018-MOXBA01

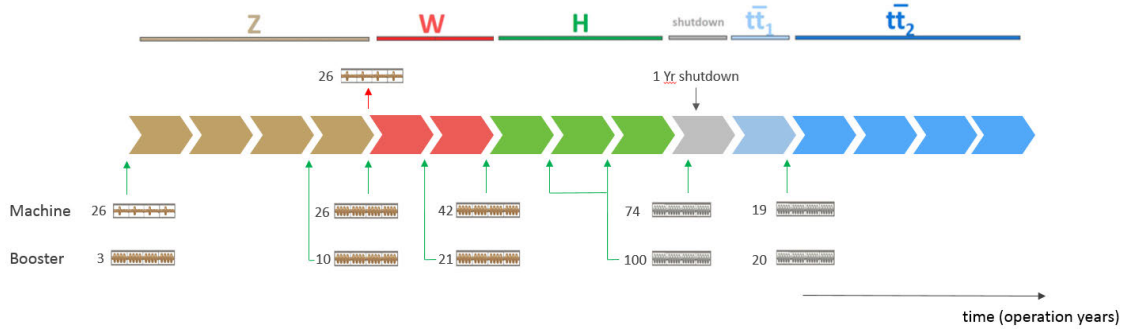

Figure 7: FCC-ee operation time line. The bottom part indicates the number of cryomodules to be installed in the collider and booster, respectively, during the various shutdown periods (O. Brunner); also see [2].

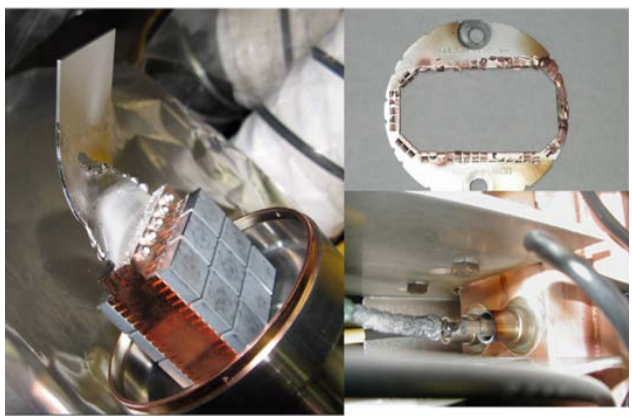

Figure 8: Photos of PEP-II spoiler, RF shield and beam-position monitor damaged by HOM heating.

10 shows, for the example of CEPC [6], that the resistive-wall contribution indeed dominates the total longitudinal short-range wake field.

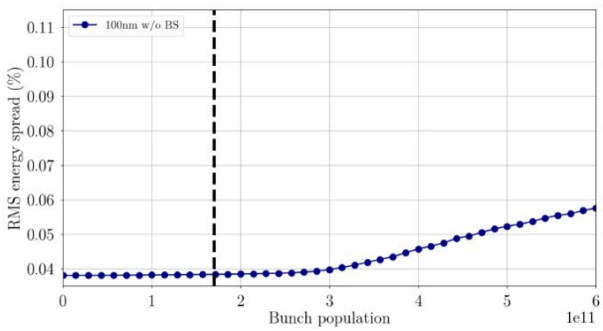

Figure 9: FCC-ee microwave instability threshold with 100 nm NEG coating on top of a copper chamber.

Resistive-wall and cavity resonances can also drive multi-bunch instabilities. For FCC-ee and CEPC the fundamental cavity mode impedance is important. The optimum cavity detuning is (minus) four revolution harmonics for FCC-ee and (minus) 6 revolution harmonics for CEPC. As a result for FCC-ee the most unstable multi-bunch mode corresponds to $m = -4$; see Fig. 11. The effective cavity impedance

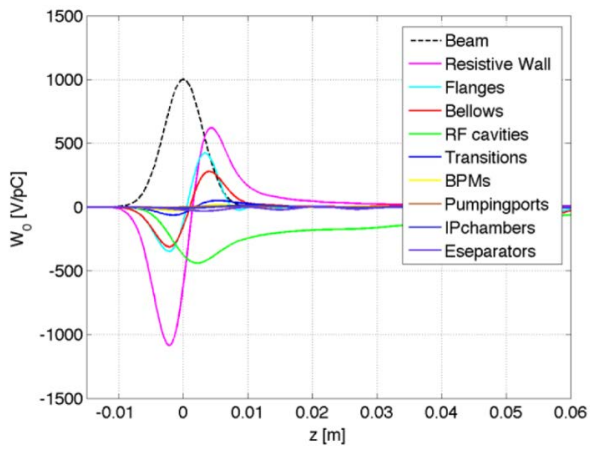

Figure 10: CEPC longitudinal partial single-bunch wake field due to various components and the total wake field [6] (N. Wang).

can be drastically reduced by strong RF feedback, as is illustrated in Fig. 12. Figure 13 demonstrates that using such feedback all coupled-bunch growth rates become weaker than the radiation damping rate.

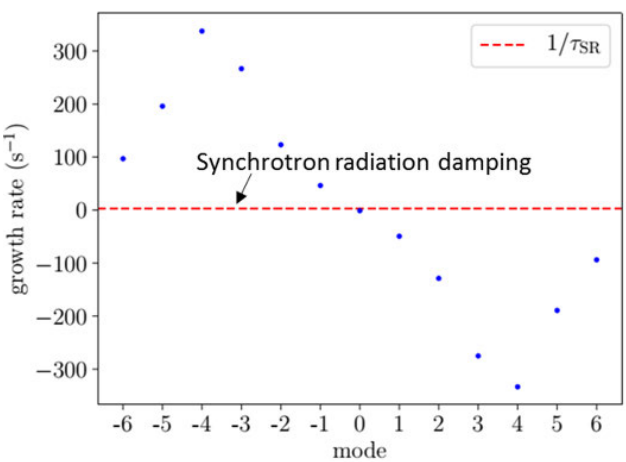

Figure 11: Longitudinal coupled-bunch growth rates without RF feedback, compared with the radiation damping rate [7].

ISBN: 978-3-95450-216-5 doi:10.18429/JACoW-eeFACT2018-MOXBA01

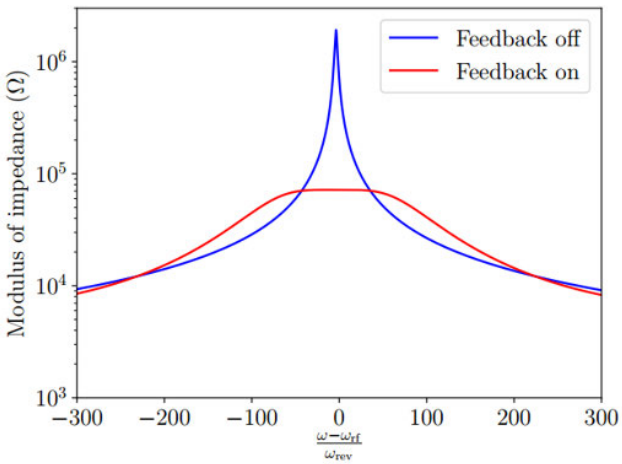

Figure 12: Cavity impedance without and with strong RF feedback [7].

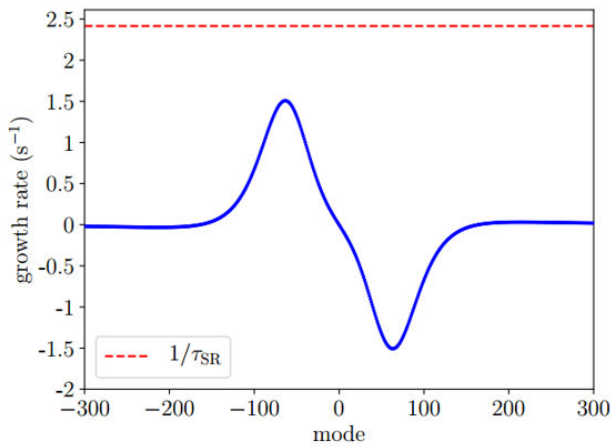

Figure 13: Longitudinal coupled-bunch growth rates with strong RF feedback, compared with the radiation damping rate [7].

Obtaining a high beam current in the positron ring requires a thorough suppression of electron-cloud formation everywhere around the ring. The countermeasures adopted for SuperKEKB [8] include (1) beam pipe with antechamber [Fig. 14 (right)], (2) rough surfaces at the primary photon impact region inside the antechamber, (3) low-SEY [TiN] coatings for 90% of the beam pipes [Fig. 14 (right)], (4) grooves inside the bending magnets [see Fig. 14 (left)], (5) clearing electrodes in the wiggler chambers, (6) solenoidal fields of about 50 G in all drift spaces, plus, finally, (7) beam conditioning. This suite of countermeasures has proven highly successful. So far at SuperKEKB no blow up of the vertical beam size has been observed for the nominal bunch spacing of two 500-MHz RF buckets (i.e. 4 ns) up to bunch currents exceeding 60% of the design value; see Fig. 15.

Yet another challenge arising from the high beam current is machine protection. Several collimators of SuperKEKB were damaged due to beam impact, already in the commissioning phase 2 [13]. The collimators of future machines should be robust enough, and be positioned sufficiently precise, to withstand any unavoidable beam impact, or, otherwise, the beam must be aborted by interlock systems before any damage can occur.

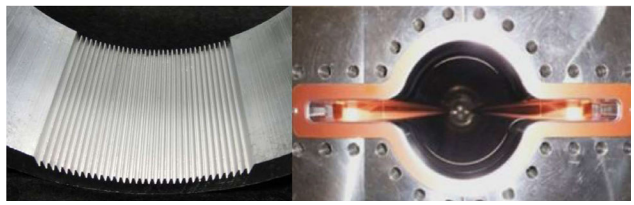

Figure 14: Anti-electron-cloud measures at SuperKEKB: grooves in bending magnets (left), and TiN coated beam pipe with antechamber (right) [8].

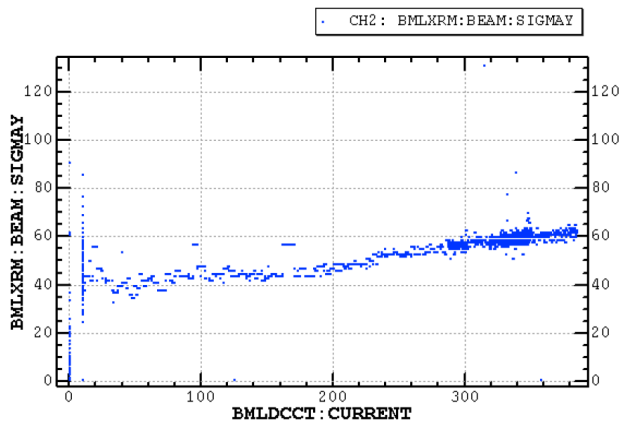

Figure 15: Vertical beam size in the SuperKEKB positron ring as a function of total beam current for a filling pattern consisting of 4 trains with 120 bunches each, and the nominal 2 bucket (4 ns) spacing (Y. Suetsugu, H. Fukuma, July 2018). No clear blow up is seen up to bunch currents of 0.8 mA (to be compared with a design value of 1.4 mA), which shows that the electron cloud density stays below the threshold of the electron-cloud induce fast head-tail instability [9, 10]. The monotonic increase of the beam at higher beam currents could either be instrumental or be caused by other effects (e.g. intrabeam scattering [11], incoherent effects of electron cloud [12], etc.).

HIGH ENERGY

One challenge related to the high beam energy is the photon energy spectrum of the synchrotron radiation. While the radiation at the Z pole (beam energy of 45.6 GeV) is easily shielded, this is no longer the case when operating as a Higgs factory or at the $t\bar{t}$ threshold (Fig. 16). Upon impact on common accelerator materials, photons of energies around 1 MeV can produce neutrons, and activate or damage accelerator components. For FCC-ee a local lead shielding mounted around dedicated discrete photon stops is foreseen; see Fig. 17.

ISBN: 978-3-95450-216-5 doi:10.18429/JACoW-eeFACT2018-MOXBA01

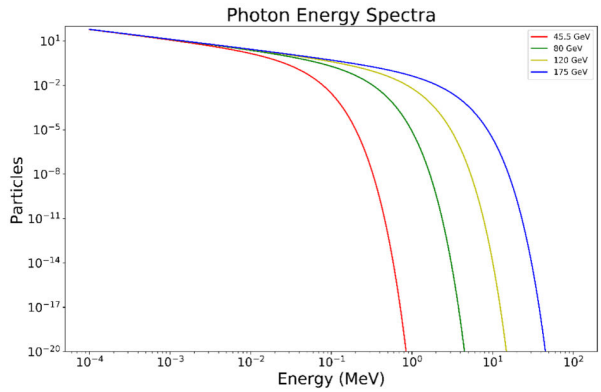

Figure 16: Synchrotron-radiation energy spectra for four different beam energies in a 100 km ring [6].

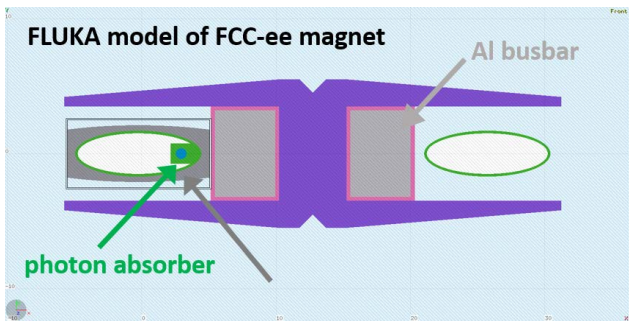

Figure 17: FLUKA model of an FCC-ee dipole magnet with lead shield integrated around the photon absorber (F. Cerutti, I. Besana).

SHORT BEAM LIFETIME

The short design beam lifetime of all future colliders, together with the high beam current, determines the particle rates for top-up operation to be provided by the injector complex. Filling the machine from zero after a failure might demand ever higher rates, depending on the filling time to be achieved. In case of the FCC-ee, this filling time is less than 20 minutes for all modes of operation.

Figure 18 shows the FCC-ee injector complex, which meets all the requirements [14, 15]. It comprises an SLC/SuperKEKB-like 6 GeV linac accelerating 1 or 2 e^+ or e^- bunches with a repetition rate of 100 or 200 Hz. The same linac is also used to accelerator other electrons for positron production at 4.46 GeV. After acceleration through the remaining part of the linac, the emittances of the positron beam are reduced in a damping ring operating at 1.54 GeV. Both electron and positron bunches at 6 GeV (end of the linac) are injected into a Pre-Booster Ring (which could be either a refurbished SPS or a new ring) and then accelerated to 20 GeV. The injection into the main top-up booster occurs at 20 GeV with an interleaved filling of e^+ and e^- for either full filling from zero or for continuous top-up.

The CEPC injector complex features a higher-energy 10 GeV linac and injects beam from the end of this linac directly into the main booster, without passing through any intermediate pre-booster. Field quality of the main booster magnets is a concern, especially at an injection energy as low as 10 GeV.

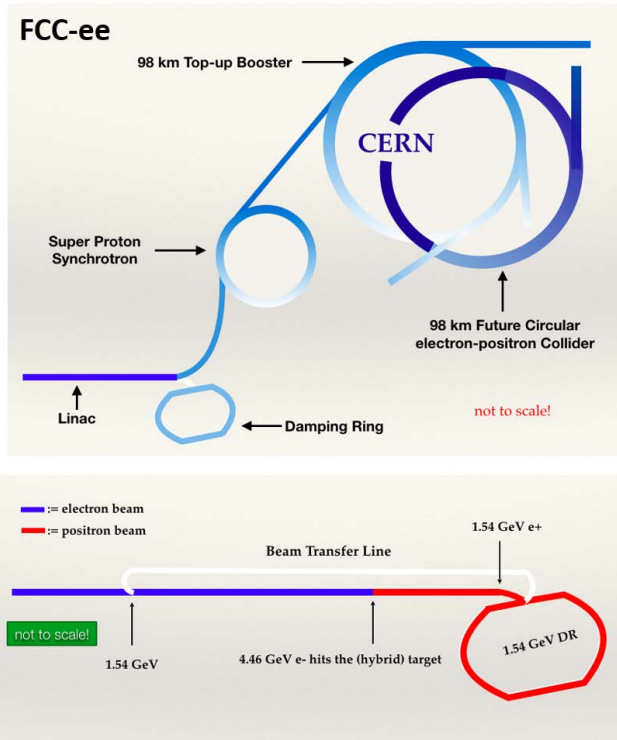

Figure 18: FCC-ee injector complex [14, 15] (S. Ogur, K. Oide, Y. Papaphilippou, O. Etisken, et al.).

The positron source is one crucial element of the injector complexes. Table 2 compares the positron production rates required for CEPC and FCC-ee with two existing (or past) sources, namely the world record SLC source (production with a 30 GeV electron beam) and the SuperKEB source.

Table 2: Positron production rates and two existing (or past) and two proposed e^+e^- colliders (I. Chaikovska, R. Chehab, P. Martyshkin, K. Oide, L. Rinolfi, Y. Papaphilippou).

coll.	CEPC	SuperKEKB	SLC	FCC-ee
e^+/sec.	10^{12}	2.5×10^{12}	6×10^{12}	10^{13}

EMITTANCE

Figure 19 illustrates that for a ring as large as the FCC-ee it should be rather straightforward to obtain the target horizontal emittance, even using a conventional FODO optics. Reaching the target vertical emittance will be more challenging. Residual coupling, spurious vertical dispersion, intrabeam scattering, electron-cloud effects, beam-ion instabilities and beam-beam related blow up will also contribute to the vertical emittance.

In particular, the beam-beam collisions can increase the vertical emittance, as is illustrated in Fig. 20. The blow up

ISBN: 978-3-95450-216-5 doi:10.18429/JACoW-eeFACT2018-MOXBA01

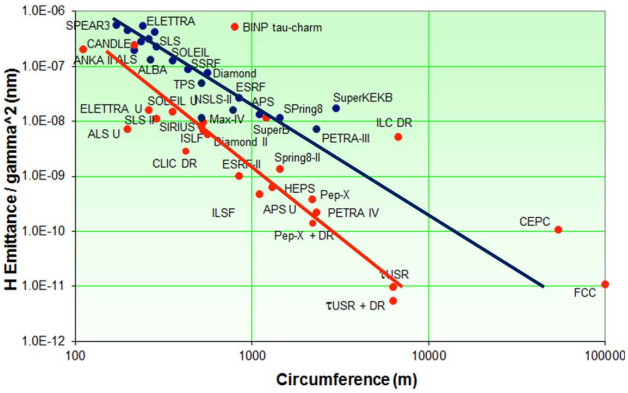

Figure 19: Emittance normalized to beam energy vs. circumference for storage rings in operation (blue dots) and under construction or being planned (red dots). The ongoing generational change is indicated by the transition from the blue line to the red line (R. Bartolini, 2016).

depends on the type of residual errors and on the working point in the tune diagram [16]. Figure 21 compiles demonstrated past and expected future emittance ratios $\varepsilon_y/\varepsilon_x$ as a function of the actual or design beam-beam tune shift, at several e+e− colliders.

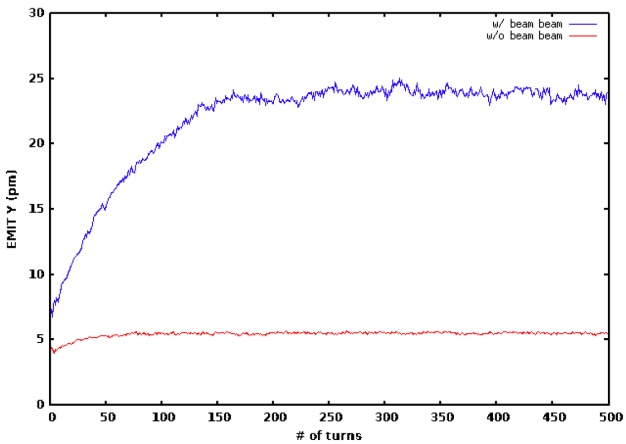

Figure 20: Example simulation of FCC-ee vertical emittance with and without collision, as a function of turn number, for one random seed (D. El Khechen, 2018).

A coherent synchro-betatron (x-z) beam-beam instability [18, 19] and 3D flip-flop effect with beamstrahlung [20] further complicate the choice of operating point, as is shown by Fig. 22.

INTERACTION POINT BETA FUNCTION

Figure 23 shows the historical evolution of the vertical interaction-point (IP) beta function at e+e− colliders. A barrier around 1 cm had been recognized by Talman, e.g. [21]. The linear collider SLC and also KEKB achieved lower values. The next great step forward will be made by SuperKEKB, with a design value of $\beta_y^* \approx 0.3$ mm, even lower than what is planned for FCC-ee or CEPC.

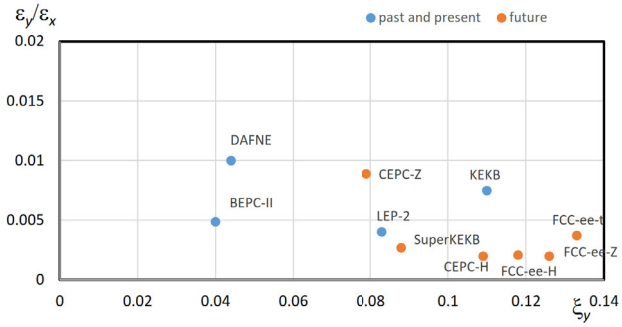

Figure 21: Vertical-to-horizontal emittance ratios achieved in various past e+e− colliders (blue) along with target values for future machines (orange) as a function of beam-beam parameter (per IP); past values were extracted from Ref. [17].

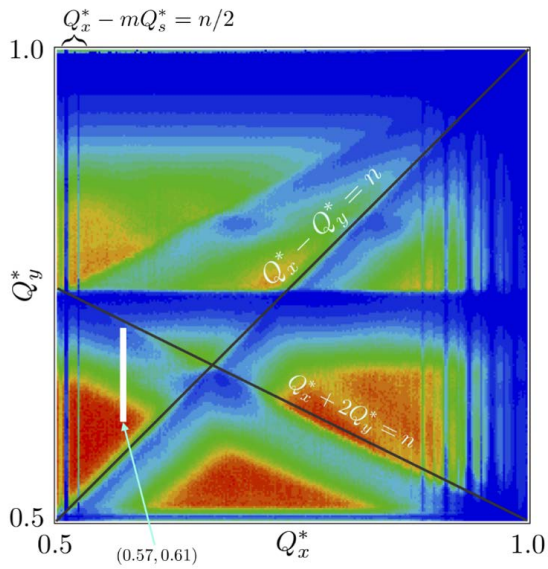

Figure 22: FCC-ee luminosity at the Z as a function of betatron tunes. The colour scale from zero (blue) to 2.3×10^{36} cm^{-2}s^{-1} (red). The white narrow rectangle above (0.57, 0.61) shows the footprint due to the beam-beam interaction. A few synchrotron-betatron resonance lines $Q_x^* - mQ_s^* = n/2$ [20].

For the FCC-ee the small beta function is accomplished with the help of a special final-focus optics, shown in Fig. 24, which complies with a multitude of constraints. This optics is asymmetric to suppress synchrotron radiation emitted towards the IP. even for $t\bar{t}$ running, the critical photon energy in the dipole magnets stays below 100 keV over the last 450 m upstream of the IP. A total of only four sextupoles (a—d), used for the local vertical chromaticity correction and for generating the crab waist, are optimized at each working point. One purpose of the sextupoles a and d is to cancel the geometric aberrations generated by the vertical-chromaticity sextupoles b and c. However, decreasing the strength of these compensating sexupoles produces the "crab waist" at the collision point. A common arc lattice is employed for all energies, with 60 degree phase advance per cell for the

ISBN: 978-3-95450-216-5 doi:10.18429/JACoW-eeFACT2018-MOXBA01

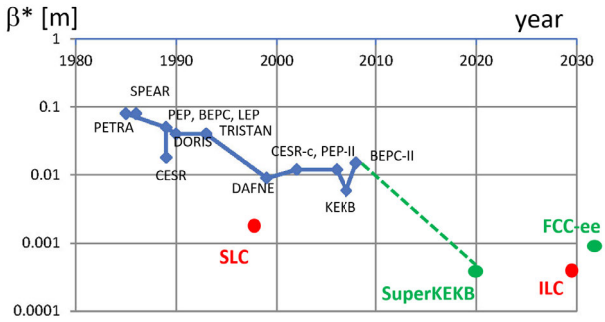

Figure 23: Vertical IP beta function for various e+e− colliders as a function of year.

Z and W running, and a more strongly focusing 90 degree for the ZH and tt̄ operation, so as to maximize stability and luminosity.

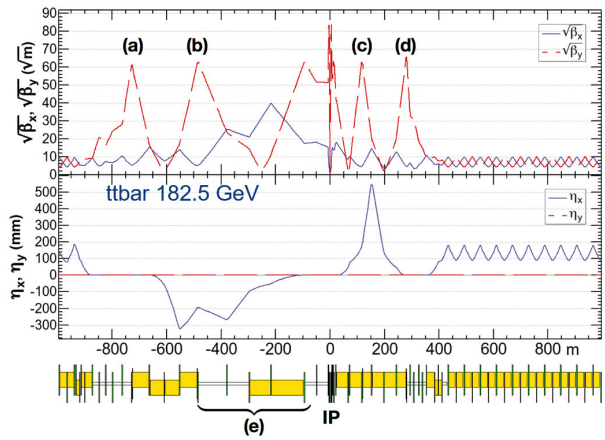

Figure 24: FCC-ee final-focus optics [22] (K. Oide). The yellow boxes indicate dipole magnets. Four sextupoles (a—d), used for the local vertical chromaticity correction and for generating the crab waist, are optimized for each working point. Common arc lattice for all energies, 60 deg for Z, W and 90 deg for ZH, tt̄ for maximum stability and luminosity

A high-quality final-focus optics is essential for obtaining an adequate dynamic aperture. An example from the CEPC design is shown in Fig. 25. The dynamic aperture can be optimized by empirically adjusting the strength of hundreds of individual sextupole pairs in the collider arcs. Efforts are ongoing to improve the dynamic aperture by particle-swarm optimization (PSO) and by training a neural network. Figure 26 illustrates the PSO process for the FCC-ee.

TOP-UP INJECTION PROCESS

The top-up injection process is essential for achieving the targeted luminosity performance. For FCC-ee, fairly "conventional" injection schemes are being considered, such as using either conventional injection or multipole-kicker schemes both on-energy and off-energy [24]. At each injection, only a few per cent of the nominal bunch charge will be transferred from the booster to the collider [24]. For

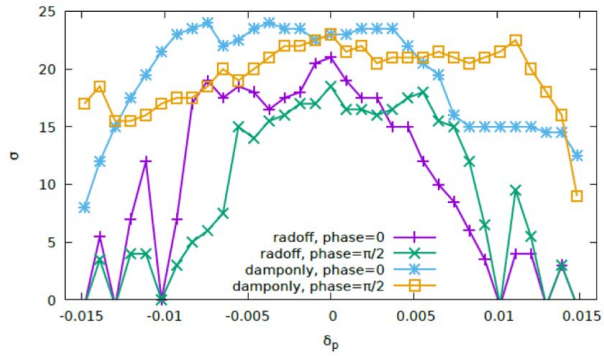

Figure 25: Off-momentum dynamic aperture for CEPC, determined by particle tracking with and without radiation damping [6].

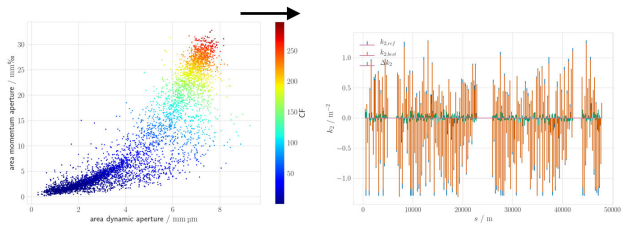

Figure 26: Particle-swarm optimization leading to enlarged momentum acceptance and transverse dynamic aperture (left), while also minimizing the strengths of the arc sextupoles (right) (T. Tydecks) [23].

CEPC a novel "swap-out" injection process is proposed, where individual bunches are first extracted from the collider ring, in order to then be merged, in the top-up booster, with lower-intensity top-up bunches, and the replenished bunches are finally sent back from the booster to the collider. This swap-out scheme is illustrated in Fig. 27

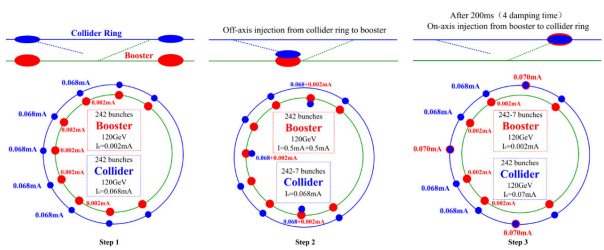

Figure 27: Swap-out injection process proposed for CEPC. [6].

SPOT SIZE

At the CERN Intersecting Storage Rings (ISR), the IP beam size was of the order of 1 mm. The rms beam sizes at the LHC are about 10 μm. The vertical beam size at the SLAC Linear Collidr (SLC) amounted to about 1 mm. Linear collier test facilities, like the SLAC FFTB and the KEK ATF-2, have achieved, at least occasionally, spot sizes between 50 and 100 nm. Similar spot sizes are also required

ISBN: 978-3-95450-216-5 doi:10.18429/JACoW-eeFACT2018-MOXBA01

for the circular colliders SuperKEKB, FCC-ee and CEPC. Future linear colliders like ILC and CLIC require spot sizes of a few nm. Table 3 presents an overview.

Table 3: RMS (vertical) spot size at various colliders and test facilities; shown in regular font are achieved values; shown in italics are design values or expected values.

collider/test facility	σ_y^* [nm]
LEP2	3500
KEKB	940
SLC	700
ATF-2, FFTB	55 (*35*), 70 (*50*)
CEPC	*60*
SuperKEKB	*50*
FCC-ee	*40*

Obtaining and maintaining the design spot size is a challenge. Succeeding in this endeavour requires regular IP aberration tuning. Figure 28 shows the increase in specific luminosity during one month of SuperKEKB phase 2 commissioning. Top-up injection and operation at constant beam current provide for rather stable conditions, which facilitate the IP tuning. Figure 29 recalls the final increase in the luminosity of the former KEKB, which was achieved by tuning skew sextupoles located in the arcs of both collider rings so as to minimize the chromatic coupling at the collision point.

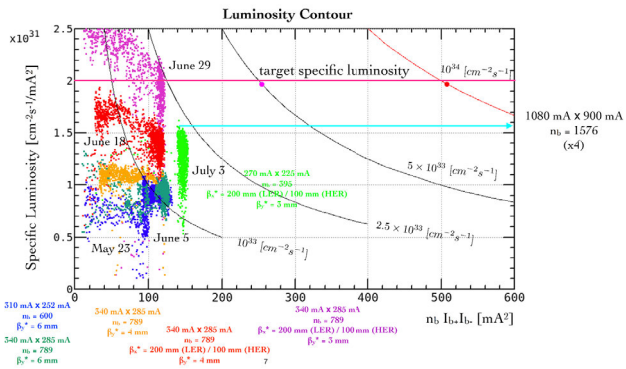

Figure 28: Improvements in SuperKEKB specific luminosity versus number of bunches and bunch current product during SuperKEKB commissioning phase 2 [13] (Y. Funakoshi).

IR QUADRUPOLES AND BEAM LOSS

The interaction region (IR) of the double-ring lowest-beta colliders contain complicated superconducting magnet systems, including corrector packages which cancel the field errors arising due to the magnets of the adjacent beam line. Figure 30 presents the intricate layout of the superconducting magnet system for SuperKEKB. Figure 31 shows a photo of the assembled superconducting magnets.

SuperKEKB experienced several quenches of the final superconducting quadrupoles in both rings) due to particle losses. It is estimated that the local loss of a few 10^3 electrons or positrons at 7 (4) GeV can quench the final quadrupole

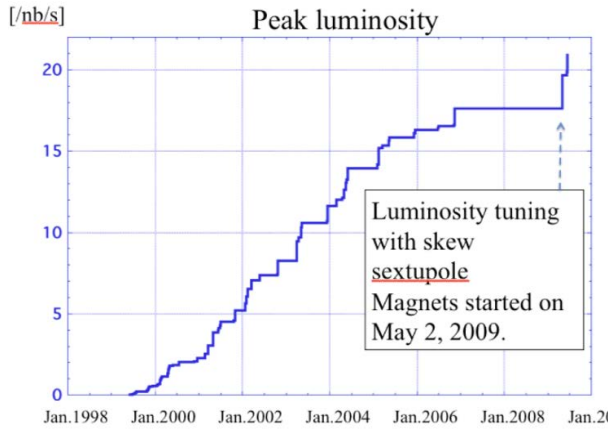

Figure 29: Peak luminosity trend since the KEKB commissioning. The peak luminosity went up significantly by tuning 20 and 8 skew sextupole magnets in the KEKB HER and LER, respectively [25] (M. Masuzawa).

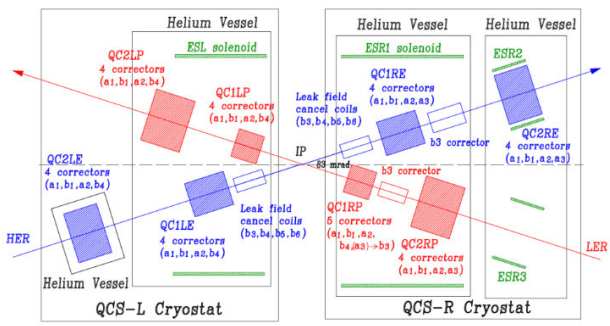

Figure 30: Layout of superconducting magnets in the SuperKEKB interaction region [26] (N. Ohuchi).

QCS [27]. The recovery time after a quench is 2–3 hours; see Fig. 32.

Simulations for CEPC in Fig. 33 indicate that the rate of particles lost due to unavoidable radiative Bhabha scattering immediately downstream of the collision point could already be close to the quench limit of the final quadrupole, if the quench level is similar to the one at SuperKEKB.

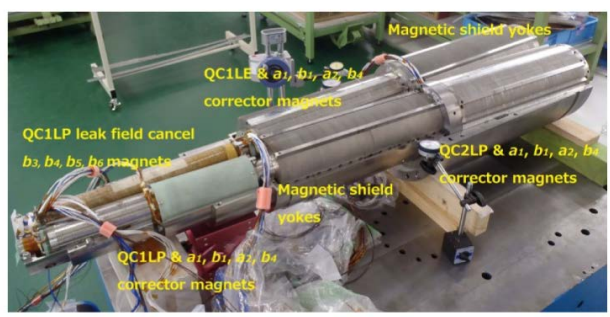

Figure 31: Assembled superconducting magnets in the front helium vessel of the "QCSL" cryostat [26] (N. Ohuchi).

ISBN: 978-3-95450-216-5 doi:10.18429/JACoW-eeFACT2018-MOXBA01

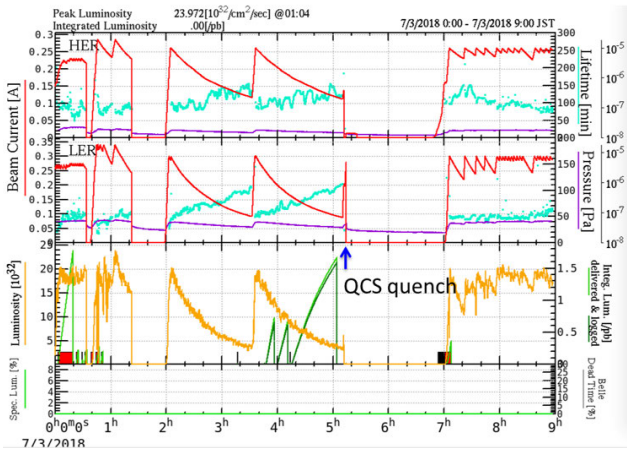

Figure 32: Two hours of downtown caused by a final-quadrupole quench at SuperKEKB during commissioning phase 2 (Y. Funakoshi).

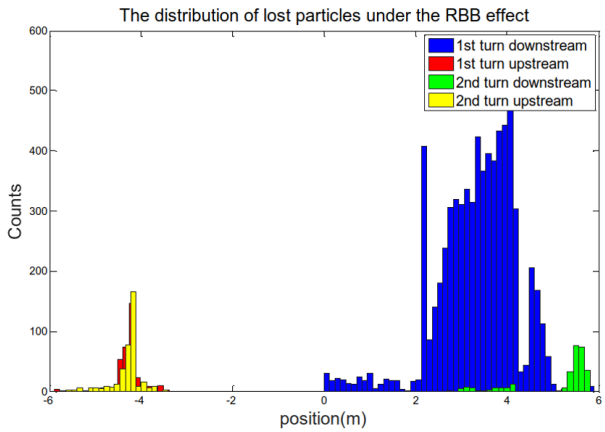

Figure 33: Simulated particles lost near the CEPC IP (at position 0) due to radiative Bhabha scattering, for a a total of 200,000 radiative Bhabha scattering events (S. Bai) [6]).

The quench limit might be significantly improved by a novel canted-cosine theta (CCT) quadrupole, which is being developed and prototyped for FCC-ee [28]; see Fig, 34. Other main advantages of the CCT quadrupole are as follows: excellent field quality (<1 unit); no need for b_3 correctors; no additional space required for any other correctors; excellent local field quality even at the edges; excellent cross-talk compensation between the two beam apertures; and cost-effective production (no pre-stress, simple winding, light construction). Magnet design and mechanical design are complete. Responses to manufacturing call were already received. The next project milestones are coil winding, impregnation, field measurement (at warm or cold), and quench training plus ultimate current studies.

POLARIZATION

A few percent of vertical polarization enables a precise energy calibration, at the 10^{-6} level, using the method of resonant depolarization [29]. Figure 35 shows that, for FCC-ee, a high level of equilibrium polarization is expected at the Z pole without any particular effort, and that dedicated spin-orbit matching will help achieve the required polarization level at the WW threshold.

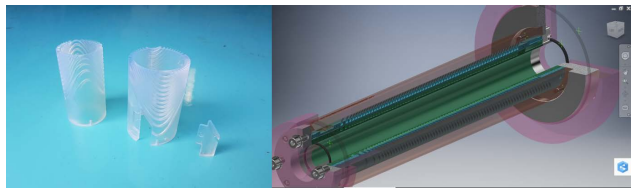

Figure 34: The FCC-ee final-focus canted cosine theta quadrupole project (M. Koratzinos) [28].

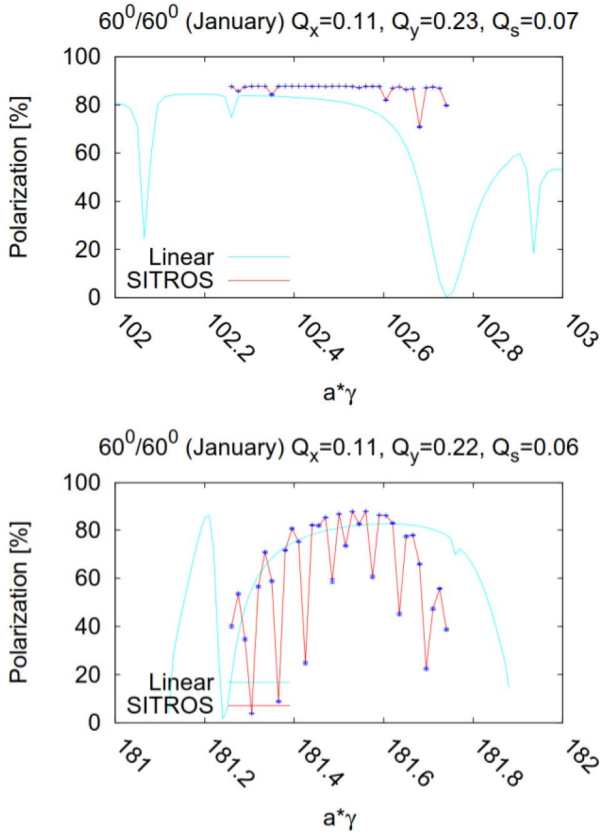

Figure 35: Polarization on the Z pole after closed-orbit correction only (top) and at the WW threshold after correcting the closed orbit, minimizing the spin-orbit coupling, correcting the betatron coupling and aligning the $\vec{n}_0$ axis (bottom) [30] (E. Gianfelice-Wendt). A linear polarization calculation (SLIM [31]) and the results of nonlinear spin tracking (SITROS [32]) are compared.

"GREEN" ACCELERATOR

The future colliders should be extremely energy efficient This is achieved, for example, by the development of highly efficient RF power sources [33] and low-power twin aperture magnets [34] (Fig. 36). Such technological improvements

ISBN: 978-3-95450-216-5 doi:10.18429/JACoW-eeFACT2018-MOXBA01

lead to the total FCC-ee electric power budgets compiled in Table 4 (also see [35]).

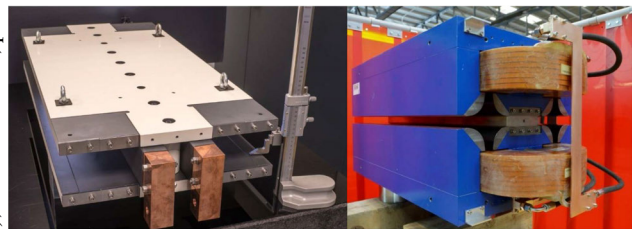

Figure 36: Photos of low-power twin-aperture dipole and quadrupole prototype magnets [34].

KEY ROLE AND OUTLOOK

A final challenge for machines like FCC-ee and CEPC is to serve as a key stepping stone towards the next hadron collider (Fig. 37). Indeed, FCC-ee/CEPC will provide (1) a 100 km tunnel, (2) the technical infrastructure (general services, cryogenics, cooling + ventilation, RF system, etc.); (3) the time (15–20 years) needed to develop and build 1000's of efficient high-field magnets, (4) additional physics motivations and a clear target energy for the subsequent pp collider.

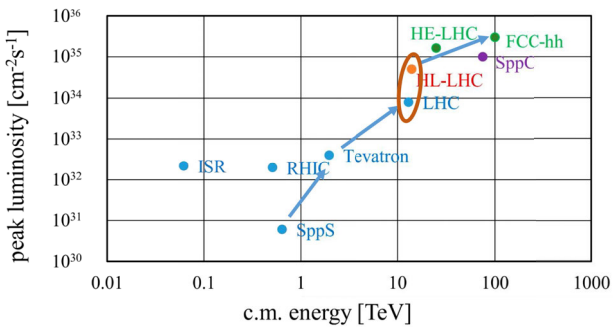

Figure 37: Past, present and proposed hadron colliders.

REFERENCES

[1] B. Richter, "Very High Energy Electron-Positron Colliding Beams for the Study of Weak Interactions," *Nucl. Instr. Methods* 136 (1976) 47–60.

[2] A. Apollonio *et al.*, "FCC-ee Operation Model, Availability, and Performance," Proc. eeFACT2018, Hong Kong (2018)

[3] A. Novokhatski,"Coherent Wave Excitation in a High Current Storage Ring," presented at *eeFACT2016*, Cockcroft Institute, Daresbury, 23–27 October 2016.

[4] I. Karpov, R. Calaga, and E. Shaposhnikova, "High order mode power loss evaluation in future circular electron-positron collider cavities," *Phys. Rev. Accel. Beams* 21, 071001 (2018).

[5] E. Belli *et al.*, "Beam dynamics effects of electron cloud and impedance with coated beam chamber in the Future Circular e+e− Collider and characterization of TiZrV thin films," submitted to PRAB (2018).

[6] The CEPC Study Group, "CEPC Conceptual Design Report," arXiv:1809.00285 (2018).

[7] R. Calaga, I. Karpov, S. Gorgi Zadeh, "RF system for FCC-ee," presentation at eeFACT2018, Hong Kong (2018).

[8] Y. Suetsugu, "Electron Cloud Effect (ECE) Mitigation Studies in SuperKEKB", Proc. eeFACT2018, Hong Kong (2018)

[9] K. Ohmi, F. Zimmermann, "Head-tail instability caused by electron cloud in positron storage rings," *Phys. Rev. Lett.* 85 (2000) 3821–3824

[10] K. Ohmi, F. Zimmermann, E.A. Perevedentsev, "Wake-field and fast head-tail instability caused by an electron cloud," *Phys. Rev. E* 65 (2001) 016502

[11] K.L.F. Bane, H. Hayano, K. Kubo, T. Naito, T. Okugi, J. Urakawa, "Intrabeam scattering analysis of measurements at KEK's Accelerator Test Facility damping ring," *Phys. Rev. ST Accel. Beams* 5 (2002) 084403

[12] E. Benedetto, G. Franchetti, F. Zimmermann, "Incoherent effects of electron cloud in proton storage rings," *Phys. Rev. Lett.* 97 (2006) 034801

[13] Y. Ohnishi, "Highlights from SuperKEKB Phase 2 Commissioning," presentation at eeFACT2018, Hong Kong (2018).

[14] S. Ogur *et al.*, "Overall Injection Strategy for FCC-ee" presentation at eeFACT2018, Hong Kong (2018).

[15] S. Ogur *et al.*, "Preliminary design of FCC-ee pre-injector complex," *Journal of Physics: Conference Series*, Volume 874, conference 1 (2017).

[16] D. El Khechen *et al.*, "Beam-beam Blowup in the Presence of xy Coupling Sources at FCC-ee," Proc. eeFACT2018, Hong Kong (2018)

[17] K.A. Olive et al. (Particle Data Group), *Chin. Phys. C*, 38, 090001 (2014) section 30.

[18] Coherent Beam-Beam Instability in Collisions with a Large Crossing Angle K. Ohmi, N. Kuroo, K. Oide, D. Zhou, and F. Zimmermann, *Phys. Rev. Lett*. 119, 134801 (2017).

[19] N. Kuroo, K. Ohmi, K. Oide, D. Zhou, and F. Zimmermann, "Cross-wake force and correlated head-tail instability in beam-beam collisions with a large crossing angle," *Phys. Rev. Accel. Beams* 21, 031002 (2018).

[20] D. Shatilov, "IP Beam Parameter Optimization for FCC-ee," *FCC Week 2018*, Amsterdam, 9–13 April 2018 (2018).

[21] R. Talman, "Scaling Behaviour of Circular Colliders Dominated by Synchrotron Radiation," arXiv:1504.01627 (2015).

[22] K. Oide et al., "Design of beam optics for the future circular collider e+e- collider rings," *Phys. Rev. Accel. Beams* 19, 111005 (2016).

[23] T. Tydecks, "First results of dynamic aperture optimisation using PSO," *78th FCC-ee Optics Design Meeting*, 7 September 2018 (2018).

[24] M. Aiba, B. Goddard, K. Oide, Y. Papaphilppou, A. Saa Hernandez, D. Shwartz, S. White, F. Zimmermann, "Top-up injection schemes for future circular lepton collider," *Nucl. Instr. Methods A*, vol. 880 (2018) 98–106; https://doi.org/10.1016/j.nima.2017.10.075

[25] M. Masuzawa *et al.*, "Installation of Skew Sextupole Magnets at KEKB," *Proc. IPAC10* Kyoto (2010) 1533.

ISBN: 978-3-95450-216-5 doi:10.18429/JACoW-eeFACT2018-MOXBA01

Table 4: Target values for average power per subsystem in different operation modes of FCC-ee, compared with the average power of LEP2 (computed, for each system, as total energy consumed in the year 2000 [36] divided by 200 days).

lepton collider	Z	W	ZH	$t\bar{t}$	LEP2
beam energy [GeV]	45.6	80	120	182.5	104
total RF power [MW]	163	163	145	145	42
collider cryogenics [MW]	1	9	14	46	18
collider magnets [MW]	4	12	26	60	16
booster RF & cryogenics [MW]	3	4	6	8	N/A
booster magnets [MW]	0	1	2	5	N/A
pre-injector complex [MW]	10	10	10	10	10
physics detectors (2) [MW]	8	8	8	8	9
data center [MW]	4	4	4	4	N/A
cooling & ventilation [MW]	30	31	31	37	16
general services [MW]	36	36	36	36	9
total electrical power [MW]	259	278	282	359	~120

[26] N. Ohuchi, "Final-focus Superconducting Magnets for SuperKEKB," *Proc. IPAC'18* Vancouver (2018) 1215.

[27] Y. Ohnishi, "Report on SuperKEKB Phase 2 Commissioning," *Proc. IPAC'18* Vancouver (2018) 1.

[28] M. Koratzinos, G.A. Kirby, J. V. Nugteren, A.R. Dudarev, "A Method for Greatly Reduced Edge Effects and Crosstalk in CCT Magnets," *IEEE Transactions on Applied Superconductivity*, vol. 28, no. 3 (2018).

[29] E. Gianfelice-Wendt, "Investigation of beam self-polarization in the future e+e- circular collider," *Phys. Rev. Accel. Beams* 19, 101005 (2016).

[30] E. Gianfelice-Wendt, private communication (2018).

[31] A.W. Chao, "Evaluation of Radiative Spin Polarization in an Electron Storage Ring," *Nucl. Instr. Meth.* 180 (1981) 29.

[32] J. Kewisch, "Simulation of Electron Spin Depolarisation with the computer Code SITROS," *DESY* 83-032 (1983). IM

[33] Andrey Yu. Baikov, Chiara Marrelli, and Igor Syratchev, "Toward High-Power Klystrons With RF Power Conversion Efficiency on the Order of 90%," *IEEE Transactions on Electron Devices*, VOL. 62, NO. 10, OCTOBER 2015 (2015).

[34] A. Milanese, "Efficient twin aperture magnets for the future circular e+/e- collider," *Phys. Rev. Accel. Beams* 19, 112401 (2016).

[35] F. Zimmermann *et al.*, "Electrical Power Budget for FCC-ee," *Proc. IPAC'16*, Busan (2016) p. 3828

[36] "Énergie Électrique, Rapport Mensuel Décembre 2000, Bilan Année 2000", *CERN internal report* (2000).